














RESEARCH ARTICLE

10.1029/2020JD033752

Observations of Ice Nucleating Particles in the Free Troposphere From Western US Wildfires

Special Section:

Fire in the Earth System

Kevin R. Barry¹ , Thomas C. J. Hill¹ , Ezra J. T. Levin^{1,2} , Cynthia H. Twohy³ , Kathryn A. Moore¹ , Zachary D. Weller⁴ , Darin W. Toohey⁵ , Mike Reeves⁶, Teresa Campos⁶ , Roy Geiss⁷ , Gregory P. Schill^{1,8,9} , Emily V. Fischer¹ , Sonia M. Kreidenweis¹ , and Paul J. DeMott¹ 

Key Points:

- Wildfires are sources of ice-nucleating particles (INPs) to the free troposphere
- INP compositions from sampled wildfires were dominated by organics
- Contributions of tar ball composition INPs evidenced a secondary formation mechanism

Supporting Information:

- Supporting Information S1

Correspondence to:

K. Barry,
Kevin.Barry@colostate.edu

Citation:

Barry, K. R., Hill, T. C. J., Levin, E. J. T., Twohy, C. H., Moore, K. A., Weller, Z. D., et al. (2021). Observations of ice nucleating particles in the free troposphere from western US wildfires. *Journal of Geophysical Research: Atmospheres*, 126, e2020JD033752. <https://doi.org/10.1029/2020JD033752>

Received 23 AUG 2020

Accepted 30 DEC 2020

¹Department of Atmospheric Science, Colorado State University, Fort Collins, CO, USA, ²Now at Handix Scientific, Boulder, CO, USA, ³NorthWest Research Associates, Redmond, WA, USA, ⁴Department of Statistics, Colorado State University, Fort Collins, CO, USA, ⁵Department of Atmospheric and Oceanic Sciences, University of Colorado Boulder, Boulder, CO, USA, ⁶National Center for Atmospheric Research, Boulder, CO, USA, ⁷Department of Chemistry, Colorado State University, Fort Collins, CO, USA, ⁸Now at Cooperative Institute for Research in Environmental Sciences, University of Colorado, Boulder, CO, USA, ⁹Now at Chemical Sciences Laboratory, National Oceanic and Atmospheric Administration, Boulder, CO, USA

Abstract Wildfires in the western United States are large sources of particulate matter, and the area burned by wildfires is predicted to increase in the future. Some particles released from wildfires can affect cloud formation by serving as ice-nucleating particles (INPs). INPs have numerous impacts on cloud radiative properties and precipitation development. Wildfires are potentially important sources of INPs, as indicated from previous measurements, but their abundance in the free troposphere has not been quantified. The Western Wildfire Experiment for Cloud Chemistry, Aerosol Absorption, and Nitrogen campaign sampled free tropospheric immersion-freezing INPs from smoke plumes near their source and downwind, along with widespread aged smoke. The results indicate an enhancement of INPs in smoke plumes relative to out-of-plume background air, but the magnitude of enhancement was both temperature and fire dependent. The majority of INPs were inferred to be predominately organic in composition with some contribution from biological sources at modest super cooling, and contributions from minerals at deeper super cooling. A fire involving primarily sagebrush shrub land and aspen forest fuels had the highest INP concentrations measured in the campaign, which is partially attributed to the INP characteristics of lofted, uncombusted plant material. Electron microscopy analysis of INPs also indicated tar balls present in this fire. Parameterization of the plume INP data on a per-unit-aerosol surface area basis confirmed that smoke is not an efficient source of INPs. Nevertheless, the high numbers of particles released from, and ubiquity of western US wildfires in summertime, regionally elevate INP concentrations in the free troposphere.

1. Introduction

Wildfires severely impact air quality in both the near and far field, with resulting implications for human, animal, and environmental health. Western US wildfires are forecasted to increase in the future (e.g., Brey et al., 2020; Flannigan et al., 2009; Liu et al., 2016; Spracklen et al., 2009; Westerling et al., 2011; Yue et al., 2013). Wildfires are a large source of particulate matter with diameters smaller than 2.5 μm and their increasing emissions have offset improvements in air quality from decreasing emissions of anthropogenic pollutants (McClure & Jaffe, 2018; O'Dell et al., 2019). They are also capable of lofting soil, plant, and ash particles by creating a zone of convergence and altering the near-surface winds (Wagner et al., 2018). Thus, they can be a source of both combusted and uncombusted material to the free troposphere. Emissions from smoke can also undergo photochemical reactions to form secondary organic aerosols downwind (e.g., Garofalo et al., 2019), which broadens the influence of fires beyond dilution of primary emissions.

This study focuses on the subset of particles released from wildfires that affect cloud formation by acting as ice-nucleating particles (INPs). INPs are necessary to initiate ice formation at temperatures above the level of homogeneous freezing (-38°C) and are important over continental regions, as ice clouds account for the majority of precipitation there (Mülmenstädt et al., 2015). INPs can have complex climatic impacts by altering cloud radiative properties, as well as affecting cloud lifetime and precipitation development though

ice indirect effects (DeMott et al., 2010; Lohmann et al., 2002). INPs may initiate freezing via several modes (Kanji et al., 2017). In super cooled clouds, the dominant mechanism is thought to be immersion freezing, wherein the INP has been incorporated into a supercooled cloud droplet and initiates freezing at some temperature characteristic of its nature. These immersion-freezing INPs have numerous sources, including mineral dust, which is thought to be the most efficient at temperatures lower than about -15°C (Murray et al., 2012), and a wide variety of organic and biological material that can initiate freezing at temperatures higher than -5°C (Hill et al., 2018).

Some previous INP measurements from biomass burning have been made in the laboratory and in the field. The second Fire Laboratory at Missoula Experiment (FLAME 2) study tested INP production from 21 different fuels characteristic of wildfires and prescribed burns in the United States and Asia (Petters et al., 2009). About two-third of burns did not produce detectable numbers of immersion freezing INPs active at -30°C ; among the fuels that did, there was large variability in both the numbers of INPs produced and the fraction of burns that produced detectable INPs for each fuel type. For example, for common western US fuels, Ponderosa pine had measurable INP concentrations in 5 of 16 burns, and sagebrush in 2 of 7 burns with >1 INP in 10^4 particles. INP measurements in the FLAME 4 study (Levin et al., 2016) also demonstrated that fires can be a potential source of INPs, but via sampling less diluted smoke, found a mean of 1 INP in 10^6 particles. Prenni et al. (2012) made primarily ground-based field measurements (one prescribed fire plume intercept at altitude) at -30°C of emissions from western US wildfires and prescribed burns and found positive correlations between INP number concentrations and total particle concentrations during flaming combustion periods. McCluskey et al. (2014) made surface-based measurements of INPs active between -12°C and -32°C in two Colorado wildfire plumes and found nearly an order of magnitude higher in-plume INP concentrations compared with those in prescribed burn plumes. The composition of sampled INPs in the wildfire plumes varied, with tar balls (viscous, spherical, organic particles; e.g., Adachi et al., 2019) largely present within one plume, suggesting a secondary INP source. However, the other plume had a larger mineral/oxide fraction, suggesting the importance of mineral dust, which was presumably from soils but also occurred within a general period of long range transport of dust into the region. More recently, Schill et al. (2020) used ground-based measurements in wildfire plumes near Boise, Idaho, to show an order of magnitude increase in INP concentrations within plumes over the background atmosphere. The INPs were deduced to be primarily organic in composition, with almost immeasurable contributions of black carbon INPs in the wildfire plumes, consistent with the laboratory results of Levin et al. (2016) for combustion of Ponderosa pine, a common western US fuel.

This work builds on previous laboratory and field measurements by providing the first free tropospheric measurements of INPs in wildfire plumes, obtained during the Western Wildfire Experiment for Cloud Chemistry, Aerosol Absorption, and Nitrogen (WE-CAN) campaign. These observations shed light on INPs from wildfires at altitudes that can readily affect cloud formation and be transported long distances. We explore the effect of the plume on ambient INP concentrations, the composition of the plume INPs, and the variability in INP emissions among fires. Information on wildfire INP evolution during atmospheric transport is achieved through several pseudo-Lagrangian plume sampling efforts.

2. Methods

2.1. WE-CAN Overview

The WE-CAN campaign was based in Boise, Idaho, during July and August 2018. Over the course of 6 weeks, 16 research flights (RF) were conducted on the NSF/NCAR C-130 aircraft to sample smoke-impacted clouds, aged smoke, and fresh plumes, resampling the latter moving downwind to study the effects of aging. For definable plumes (those attributable to a specific fire), the plane initially flew behind the fire to characterize background air; this initial maneuver was followed by repeated plume transects away from the fire perpendicular to the wind direction, with additional background measurements between transects. Although near-source characterization and Lagrangian sampling (i.e., resampling of the same plume element as it was transported downwind) were attempted for most smoke plumes associated with a specific known fire, flight restrictions and plume location uncertainties often interfered. Hence, we refer to the measurements as pseudo-Lagrangian. Table 1 details the flights and corresponding plumes that represent

Table 1
Details of the Plumes Sampled During WE-CAN That Were Analyzed in Detail for INP properties

RF (#)	Date	Fire name/description	Fire location	Altitude range (m ASL)
2	July 26, 2018	Carr Fire	CA	3,409–3,871
3	July 30, 2018	Taylor Creek Fire	OR	3,342–3,720
4	July 31, 2018	Sharps Fire	ID	5,114–5,153
5	July 30, 2018	<i>River of Smoke</i>	CA, OR, ID	1,330–4,128
6	August 4, 2018	Kiwah/Rabbit Foot Fires	ID	3,658–4,283
7	August 6, 2018	Donnell Fire	CA	4,216–4,556
8	August 8, 2018	<i>Central Valley Boundary Layer</i>	CA	133–2,441
9	August 9, 2018	Dollar Ridge/Coal Hollow Fires	UT	4,221–4,539
9	August 9, 2018	Bear Trap Fire	UT	4,527–4,557
11	August 15, 2018	Shellrock Fire	MT	3,156–3,199
13	August 20, 2018	Mendocino Complex Fire	CA	3,037–4,625
15	August 26, 2018	South Sugarloaf Fire	NV	3,658–4,609

Notes. The altitude range is given as meters above sea level for the portion of the flight with CFDC data. Flights with a pseudo-Lagrangian sampling strategy are bolded. Flights sampling regional aged smoke, with no single identified fire source, are shown in italics.

Abbreviations: INP, ice-nucleating particle; WE-CAN, Western Wildfire Experiment for Cloud Chemistry, Aerosol Absorption, and Nitrogen.

the best cases for INP measurements, with italicized fire names indicating flights that sampled regional, aged smoke. Their spatial locations are shown in Figure 1. A departure from the typical pseudo-Lagrangian strategy was implemented for the South Sugarloaf Fire plume in RF15, with transects at multiple altitudes at one downwind location before moving on to the next. Up to four altitudes were sampled at each location (from approximately 3,600 to 4,600 m ASL), and repeated locational measurements were separated by approximately 2–4 h. The Continuous Flow Diffusion Chamber (CFDC) captured samples from transects ranging from 30 to 100 km from the fire center.

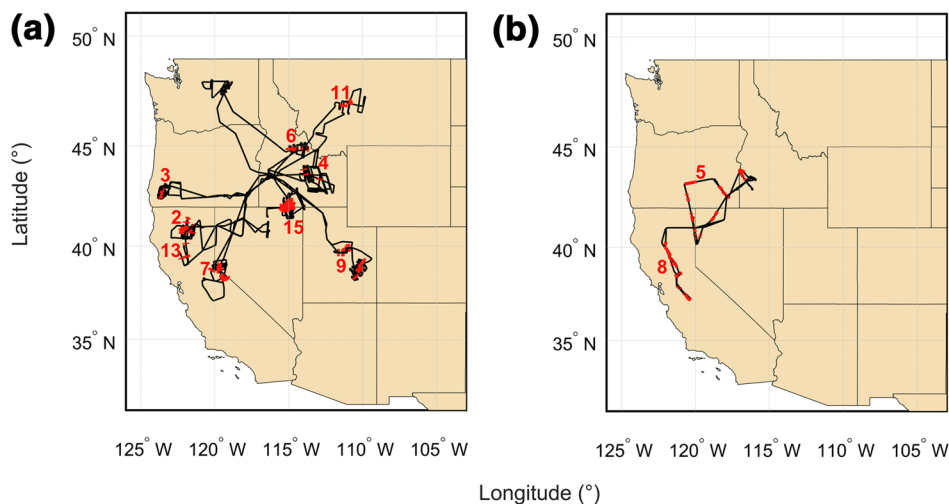


Figure 1. The locations of INP samples (red), for (a) samples attributable to definable plumes and (b) in aged smoke, overlaid on the flight tracks in black. Red numbers indicate RF numbers listed in Table 1. INP, ice-nucleating particle; RF, research flights.

2.2. INP Measurement Techniques

2.2.1. Ice Spectrometer for Offline INP Analysis

The Colorado State University (CSU) Ice Spectrometer (IS) is a laboratory-based instrument that analyzes liquid suspensions from filter samples for INPs, acting in the immersion freezing mode (where the INP is first immersed in the liquid phase before initiating freezing; Kanji et al., 2017). The present version, used for this work, is described in DeMott et al. (2018). Aerosol filter samples were collected on the NSF/NCAR C-130 with two 47-mm diameter, in-line aluminum filter holders with precleaned, 0.2- μm pore diameter Nuclepore polycarbonate filter membranes. Ambient aerosol particles were transported into the cabin through the NCAR Solid Diffuser Inlet (SDI), based on the University of Hawaii SDI (Clarke et al., 2004; Huebert et al., 2004). The SDI flow rates resulted in super-isokinetic sampling at the exterior inlet tip, with implications for reduced particle transmission efficiencies at some sizes (Table S2): the SDI efficiency dropped below 50% for particles with diameters larger than about 4 μm , and thus none of the instruments sampling from the SDI inlet could capture particles larger than this. Additional particle line losses combined with the inlet efficiencies resulted in transfer percentages of 88%, 55%, and 24% at sizes of 1, 3, and 5 μm aerodynamic diameter, respectively, for the CFDC, and 84%, 39%, and 1.5% at sizes of 1, 3, and 5 μm aerodynamic diameter, respectively, for the IS. Corrections for losses are not made to the INP concentration data, since the sizes of INPs at varied processing conditions are unknown, but we note that effectively, our INP instruments characterized particles smaller than about 3 μm . Plume and background air filter collection times were selected using onboard, real-time carbon monoxide (CO) measurements, measured with the Aerodyne quantum cascade laser instrument (CS-108 miniQCL; Lebegue et al., 2016). The real-time CO data were used to select exposure times for switching sampling between the in-plume and background filters, and thus dictating the volumes of air passed through each (typically a few hundred standard liters for each sample: Table S1), resulting in one integrated in-plume sample per flight, matched with one integrated background sample. Thus, these samples do not capture any information on the evolution of INPs with time and distance, but reflect the average nature of INPs in the sampled portions of that plume. Mass flow rates were recorded at 1 Hz intervals to tabulate total volume filtered. Filter samples were placed into sterile 50 mL Falcon polypropylene centrifuge tubes after collection (Corning Life Sciences) and stored and transported frozen until they were analyzed at CSU.

Seven milliliters of 0.1 μm -filtered (Whatman Puradisc, PTFE membrane) deionized (DI) water were added to each tube and placed in a Roto-Torque rotator (Cole-Parmer) for 20 min to create a suspension. Thirty-two aliquots of 50 μL of each sample were then dispensed into PCR trays (OPTIMUM[®] ULTRA Brand from Life Science Products) and placed into aluminum blocks in the IS. All runs were initiated at a temperature of 23°C, with samples subsequently cooled at a rate of approximately 0.33°C min⁻¹. The freezing of wells was detected by a CCD camera, and the corresponding temperature recorded with a LabVIEW interface. The lowest temperature achievable for assessing sample INPs is defined as the temperature for which the number of sample wells frozen significantly exceeds those frozen in a 32-well, 0.1 μm -filtered, DI water negative control. This was generally between -27°C and -30°C for the samples analyzed here. Cumulative INP concentrations were determined by first calculating the INPs per milliliter of sample liquid based on Vali (1971) and converting to concentration per standard liter of air using the volume of air collected for each sample. The number of INPs from the average of seven blank filters that were handled and processed identically to the samples, with exception of air flow, were subtracted from the calculated number of INPs on each sample filter before conversion to concentration (Figure S1). This sometimes resulted in cumulative INP concentrations decreasing with lower temperatures (especially during the sampling of cleaner air or for shorter periods of time), which is an artifact of the correction. Two-tailed, 95% confidence intervals for binomial sampling were calculated based on Agresti and Coull (1998). The limit of detection was taken as the uncorrected lower 95% confidence interval for one frozen well, which considers the volumes of the droplets, suspension, and air passed through the filter. Peroxide digestions and thermal treatments were done on select filter suspensions to provide insight into INP compositions. The heat treatment warmed the suspensions to 95°C for 20 min to denature heat-labile organics, such as proteinaceous INPs. Hydrogen peroxide (H₂O₂) digestion removed all organic carbon INPs from samples following methods detailed in McCluskey et al. (2018) and Suski et al. (2018). The differences between the INP temperature spectra before and after treatment determined the proportion of each INP type in the original sample. Significance testing

between untreated and treated spectra and plume and out-of-plume background filters was performed by using a paired *t*-test over interpolated temperature intervals.

2.2.2. Continuous Flow Diffusion Chamber for Online INP Analysis

The CSU CFDC instrument (DeMott et al., 2015; Rogers, 1988; Rogers et al., 2001) consists of two concentric cylinders, an outer and inner wall, that have gradients in temperature and water vapor between them. The temperatures of the ice-coated walls determine the supersaturation profiles in the chamber with respect to ice and water. Sample air from outside the aircraft was brought in at 1.5 volumetric liters per minute taken from the SDI inlet interior line and first passed through diffusion driers. A pair of upstream impactors removed dry particles larger than 2.5 μm diameter (50% aerodynamic cut-size diameter) before the sample entered the chamber. For this study, water supersaturation in the chamber was typically held between 4% and 8% to initially encapsulate sampled particles into water droplets, emphasizing measurement of ice nucleation in the immersion freezing mode for consistency with the IS data. Total residence time during which ice nucleation could occur (chamber growth section) was approximately 5 s. Ice crystals continued to grow, and water droplets decreased toward their original dry particle sizes over an additional 2.5 s of exposure to water subsaturated conditions (chamber evaporation section) prior to detection of ice crystals by their larger sizes ($>4 \mu\text{m}$) using an optical particle counter (DeMott et al., 2015). The operating temperature of the aerosol lamina was generally kept around -25°C or colder as the INP concentrations were typically below detection limits at warmer temperatures during free tropospheric sampling. Ice crystals $>3.8 \mu\text{m}$ (50% aerodynamic cut-size diameter) exiting the CFDC chamber were collected onto grids using a single jet impactor (McCluskey et al., 2014) for subsequent analysis by scanning transmission electron microscopy/energy dispersive X-ray spectroscopy (STEM/EDX) to determine the elemental composition of individual plume INPs (see Section 2.2.4).

The time spent in plume versus in out-of-plume air was defined by using CO mixing ratios from the CS-108 miniQCL, as described above. Samples collected within individual plume intercepts were attributed to specific fires by using defined overall sampling times for each plume from the US Forest Service. Plume intercepts were then broken up into 1 min data periods, applying a minimum threshold of 30 s of useable data for the sample to be retained for inclusion in subsequent analyses; unless otherwise specified, all CFDC data shown are for these individual 1 min samples. All out-of-plume periods for each defined smoke plume, irrespective of distance downwind, were combined in order to improve statistical significance over the instrument's background to obtain a representative sample of INP concentrations in the air outside of the plume. The physical age for each plume sampling period was estimated by dividing the average distance from the fire center by the average wind speed from onboard the NSF/NCAR C-130. Uncertainties in the active burn location, friction, and entrainment, along with variable winds, may cause this estimate to deviate from the true physical age.

Approximately every 10 min during the research flights, the CFDC sample flow was filtered (HEPA) for 5 min to provide instrument background counts, which allows for quantification of artifact ice crystals from low level frost emission during operation (DeMott et al., 2017). INP concentrations, calculation of confidence intervals, and inference for differences for each sampling period were determined based on a Poisson model for rates of detection of INP-sized particles during ambient sample and surrounding filtered air periods (described in Text S1). Note that these methods represent a modification of procedures used to define these parameters in CFDC studies prior to and including Levin et al. (2019). Differences between sample periods (i.e., in plume vs. out-of-plume) were determined in the same manner.

The effects of water vapor depletion in the CFDC chamber have previously been analyzed as a function of the total aerosol number concentration (N), showing a decrease in the fraction of particles activating as INPs with increasing N (Levin et al., 2016). Since vapor depletion would lead to a potential underestimate of INPs in the plume, all CFDC data were corrected following the sigmoidal function in Levin et al. (2016), assuming no effect until N reaches $10,000 \text{ cm}^{-3}$. Values of N were obtained from a combination of the nano-Scanning Mobility Particle Sizer (nSMPS), sampling from the SDI inlet, and the wing-mounted Passive Cavity Aerosol Spectrometer Probe (PCASP), which collectively measure particle number concentrations over a diameter range from approximately 10 nm to $\sim 3 \mu\text{m}$.

2.2.3. Computation of the Surface Active Site Density Parameter

An INP normalization method that has been used previously is the calculation of the surface active site density parameter (n_s) (DeMott et al., 1995; Niemand et al., 2012), in which INP number concentrations are divided by the aerosol surface area for specific compositions. For example, n_s has been used to describe the number of ice nucleating sites carried by specific types of aerosols such as desert dust and soot measured in the laboratory (Ullrich et al., 2017), and for particles in clean marine air (McCluskey et al., 2018). This approach assumes that nucleation is a surface phenomenon, and that variability in INP concentrations for a specific particle type is due solely to aerosol size distribution differences. In this case, we define all particles in the plume as smoke. For the WE-CAN data, surface area concentrations were derived from aerosol size distributions measured by the PCASP instrument, which counts and sizes particles via their scattering signal. The nominal detected size range, based on standard calibration with polystyrene latex particles, covers $\sim 0.1\text{--}3\ \mu\text{m}$ in diameter. A standard live-time coincidence correction (Kupc et al., 2018) was applied. For most flights, PM1 (particulate matter less than $1\ \mu\text{m}$ diameter) volume concentrations deduced from the measured size distributions were linearly correlated with aerosol mass concentrations from the Aerosol Mass Spectrometer (AMS; Garofalo et al., 2019). Assuming an aerosol density of $1.5\ \text{g cm}^{-3}$ led to good agreement between the two data sets, with only a few flights suggesting increases of about 10% in particle diameter (30% in volume) in order to match the AMS data. The corresponding uncertainty in surface area concentrations is in general agreement with the quantified data uncertainties reported by Kupc et al. 2018: (Table S3) for the UHSAS optical particle probe, and we therefore use the PCASP data with the calibrated bin limits and conservatively estimate the uncertainty in surface area as 30%. We note that we have applied a spherical equivalent assumption in this calculation of surface area, whereas smoke plume particles may come in a variety of shapes and could include aggregate particles with interior surface area that would be unaccounted for. However, in the next section, we describe single particles analyses from a specific flight for which the majority of plume particles were found to have a round shape and predominately organic compositions, without significant inclusions (i.e., aggregate and fractal particles such as soot were extremely rare). Thus, we acknowledge the possibility that we have underestimated surface area by an unknown, but likely small amount in using the PCASP data in this manner. For INP data normalization, total measured aerosol surface area concentrations were averaged over the corresponding IS filter sampling periods. For CFDC data, since the instrument operated with a $2.5\ \mu\text{m}$ aerodynamic diameter cutpoint inlet, aerosol surface area concentrations were summed to $2\ \mu\text{m}$ (the estimated cutpoint physical diameter) over the corresponding CFDC sample periods. Surface area distributions computed from the combined SMPS-PCASP data suggest that very little aerosol surface area was outside the range of these instruments, which matches well the range of particle sizes efficiently sampled by the IS and CFDC. We note that we cannot exclude the possibility that some particulate surface area in the plume may have been contributed by large ($>5\ \mu\text{m}$ diameter) ash, soil, or other emitted aerosols, and has not been accounted for in this analysis.

2.2.4. Investigation of Aerosol and INP Composition

Individual particles in samples of both total aerosol and INPs were analyzed by STEM/EDX to obtain information on the particle elemental chemical composition, morphology, and mixing state. A custom two-stage impactor with approximate 50% cut sizes of 0.55 and $0.13\ \mu\text{m}$ physical diameter (assuming particle densities of $1.5\ \text{g cm}^{-3}$ at $1,000\ \text{mb}$) was used to periodically collect aerosol particles $>0.55\text{--}5\ \mu\text{m}$ and between 0.13 and $0.55\ \mu\text{m}$ (assuming particle densities of $1.5\ \text{g cm}^{-3}$ at $1,000\ \text{mb}$) from inside and outside of wildfire plumes from the SDI inlet on the C-130. Typical in-plume sampling times were $4\ \text{min}$ with a flow rate of $2.4\ \text{L min}^{-1}$ from the SDI. Although this flow results in sub isokinetic sampling into the impactor line with respect to the SDI interior tube flow, little influence is expected in the $0.13\text{--}0.55\ \mu\text{m}$ size range of the smaller cut-size impactor, and only data from the grid collected in this impactor is used in this paper. Line residence time to the impactors from the SDI was approximately $1\ \text{s}$ through smooth curving tubing, and so there should be no other size-dependent losses. Aerosol and INP impactors were fitted with $3\ \text{mm}$, 200 mesh Ni or Cu support, C/formvar coated grids (SPI Supplies, West Chester, PA).

Grids with ambient particles and CFDC INPs were subsequently analyzed at CSU on a JEOL JEM-2100F $200\ \text{kV}$ scanning transmission electron microscope with an energy dispersive x-ray spectrometer (Oxford

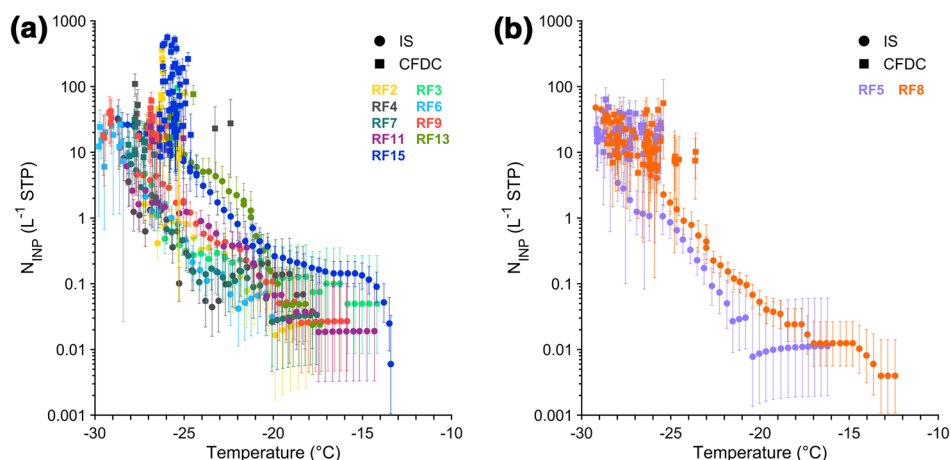


Figure 2. INP number concentration versus temperature for the plume IS (circles) and CFDC (squares) data, colored by research flight for (a) definable plumes and (b) aged smoke samples. Error bars represent 95% confidence intervals. CFDC, Continuous Flow Diffusion Chamber; INP, ice-nucleating particle; IS, Ice Spectrometer.

Energy Max 80) system. Blank grids (installed, but not exposed to sample flow) were analyzed for exclusion of potential artifacts, and background x-ray elemental spectra were obtained from particle-free regions of sampled grids to set detection limits. Approximately 50 particles from each aerosol and INP grid were imaged and analyzed for contained elements. Size, roundness (Equation 1), and other shape parameters were calculated through Fiji image processing software, which fits an outline to each particle. Particles were categorized based on spatial mapping of their detected elements (see Text S4) and morphology. Categories were Organics—other, Organics—tar balls, Mineral/Metal Oxides, and Sulfates. Mineral/Metal Oxides may contain elevated levels of Al, Ca, Fe, Mg, and Si. Sulfates includes sulfuric acid and ammonium sulfate/bisulfate (S and O only). Organic carbon content was inferred based on C signal concentration well above the surrounding substrate background and was distinguished from elemental carbon on the basis of morphology and the presence of oxygen. Tar balls were defined through their having high stability under the beam, a minimum roundness value of 0.8, a relatively uniform distribution of C, O, and N (Adachi et al., 2019), and possible smaller amounts of S, K, Cl, and Si (Pósfai et al., 2004), with a maximum of one visible inclusion. For comparisons with the aerosol second stage impactor grids, INP analysis was restricted to particles under 500 nm in diameter, which is within the range of tar ball sizes (e.g., Pósfai et al., 2004). This size restriction represented 90% of collected particles on this stage. It was also the case that 80% of INPs has spherical equivalent particle sizes in this size range for the CFDC operating conditions applied.

$$\text{Roundness} = \frac{4[\text{Area}]}{\pi[\text{Major axis}]^2} \quad (1)$$

3. Results and Discussion

Cumulative INP concentrations from 10 definable (and therefore fresher) smoke plumes (2 from RF9) and 2 regionally aged smoke flights (unattributable to any specific source; RF5 and RF8) are presented in Figure 2. Examples of total aerosol number concentrations, INP number concentrations, and CO mixing ratios from a series of plume intercepts during one flight are shown in Figure S3. The INP concentrations for the CFDC real-time measurements generally agree with those from the filters analyzed with the IS for aged smoke (Figure 2b), while many definable plume samples show higher concentrations with the CFDC (Figure 2a; Figure S4). For example, at the average CFDC processing temperature in RF8, the CFDC measured INP concentrations of 17.2 L^{-1} while the IS measured 8.99 L^{-1} , while RF2 had an average of two orders of magnitude difference (Tables 2 and 3). These differences likely arise due to the ability of the CFDC to capture small-scale plume variability (e.g., Figure S3), while the aerosol filter collections integrate across the entire plume with time and distance and potentially include noncoincident passes. Better agreement with

Table 2

Number of 1-Min CFDC Plume Segments, Average INP Concentration, and Processing Temperatures for the Plume and Out-of-Plume Background Air, and Percentage of Segments Above Plume-Background at the 95% Confidence Level for Sampled Plumes Associated With Each Research Flight

RF #	Plume segments (#)	Average plume N_{INP} (L^{-1} STP)	Average plume-background N_{INP} (L^{-1} STP)	Average plume processing T ($^{\circ}\text{C}$)	Average plume-background processing T ($^{\circ}\text{C}$)	Segments above plume-background (%)
2	24	68.9	11.5	−25.8	−24.9	46
3	7	39.2	1.3	−25.5	−25.5	100
4	7	42.4	BDL	−26.3	−25.9	100
5	71	21.4	N/A	−27.4	N/A	N/A
6	10	16.8	6.9	−29.2	−29.2	60
7	14	14.9	3.7	−27.5	−27.6	93
8	61	17.2	N/A	−26.8	N/A	N/A
9	24	27.5	12.3	−27.4	−27.6	58
11	4	20.2	10.8	−26.0	−25.1	50
13	4	42.2	9.9	−25.5	−25.7	100
15	51	123.6	5.8	−25.6	−25.7	96

Notes. N/A indicates a flight that did not have an out-of-plume background period and BDL is below the CFDC detection limit. STP is defined at 0°C and 1,013 mb.

Abbreviations: CFDC, Continuous Flow Diffusion Chamber; INP, ice-nucleating particle

the aged smoke is likely due to it being more spatially homogenous. While there are inherent discrepancies between the offline versus online collection and analysis methods (DeMott et al., 2017), they should be seen as complementary techniques for representing INPs.

Table 3

IS Plume and Out-of-Plume Background INP Concentrations at the Average CFDC Processing Temperature (See 2) and at -25°C

RF #	Plume N_{INP} (L^{-1} STP at T_{CFDC})	Background N_{INP} (L^{-1} STP at T_{CFDC})	Plume N_{INP} (L^{-1} STP at -25°C)	Background N_{INP} (L^{-1} STP at -25°C)
2	0.84	BDL	0.82	BDL
3	0.52	BDL	0.34	BDL
4	1.30	0.07	0.24	0.01
5	2.15	N/A	0.84	N/A
6	28.38	N/A	0.52	N/A
7	3.62	BDL	0.40	BDL
8	8.99	N/A	1.68	N/A
9	4.51	0.16	1.65	0.34
11	1.45	1.35	1.22	1.27
13	10.92	6.21	9.23	4.85
15	8.92	2.23	7.61	1.39

Notes. N/A indicates a flight that did not have an out-of-plume background period, no filter collected, or no data available at the corresponding temperature and BDL is below the IS detection limit. STP is defined at 0°C and 1,013 mb.

Abbreviations: CFDC, Continuous Flow Diffusion Chamber; INP, ice-nucleating particle; IS, Ice Spectrometer.

3.1. INPs in the Plume

Next, we compare INP concentrations sampled in each plume with those in the air measured outside the plume (out-of-plume “background”) at similar altitudes to evaluate evidence for enhanced INP concentrations in plume. Beginning with the CFDC measurements, the 1 min plume segments compared to the combined out-of-plume background reveal that for most flights, the majority of plume periods have INP concentrations enhanced above background. The most notable example is RF15, for which 96% of the 51 plume segments were elevated at the 95% confidence level (Table 2). RF3 and RF4 also show strong enhancements, with RF3 having a mean thirty-fold increase of INPs in the plume over background. Table 2 shows that while the average plume INP concentrations are elevated above their out-of-plume background in every flight, the enrichment varies from less than a factor of two (RF11) up to two orders of magnitude higher (RF15). The INP concentrations measured in the free troposphere in WE-CAN also agree well with previous ground-based studies. For example, McCluskey et al. (2014) found mean INP concentrations of 40 L^{-1} STP at -27°C measured in smoke around 30 km from the Hewlett Wildfire, which is within the mean values found in WE-CAN plumes at similar processing temperatures (Table 2).

The aerosol filter suspensions analyzed with the IS paint a similar picture of plume enrichment of INP concentrations, despite lower number concentrations overall (Table 3, Figure S4). The temperature of freezing

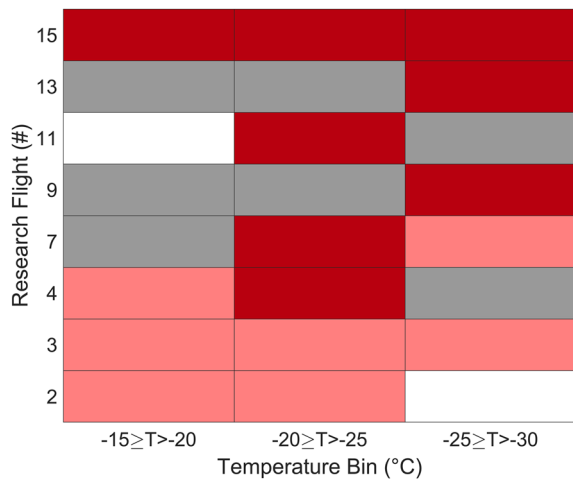


Figure 3. Heatmap indicating results of statistical testing for in-plume versus out-of-plume background INP concentrations from IS analyses. Dark red represents an increase over background at 95% confidence, light red represents an increase over background for samples where the IS background measurement was below detection limit, gray represents no difference at 95% confidence, and white indicates missing data. INP, ice-nucleating particle; IS, Ice Spectrometer.

of the first frozen IS well for the plume filters is generally several degrees higher (mean -16.2°C and range -12.4°C to -20.1°C) than for coincident out-of-plume background filters (mean -19.2°C and range -17.2°C to -24.2°C), with comparable volumes of air (Table S1). Figure 3 presents a heatmap of the results of statistical testing for a difference (95% confidence) between in- versus out-of-plume background in three temperature bins (over which most data were obtained), revealing that the level of INP enhancement differs with temperature. Some plumes sampled (RF3, RF15) were above the background across the entire temperature range. Other cases (RF7, RF9, and RF13) only had an increase in the lower temperature range. The IS data thus reveal a variable temperature-dependent picture.

While the general enhancements of INPs in plumes indicate that wildfires can perturb free tropospheric INP concentrations, this metric gives no indication of the effectiveness of wildfires as a source of INPs. Normalization of INP concentrations by surface area (n_s), when compared to similar previous parameterizations of surface active site density versus temperature for clean marine aerosols (McCluskey et al., 2018), black carbon from biomass burning (Schill et al., 2020), and desert dust (Ullrich et al., 2017), reveals the relative efficiency of wildfire smoke INPs in comparison to these other INP source types (Figure 4). The plume measurements from the CFDC are up to four orders of magnitude lower, while the IS data are up to five orders of magnitude lower than the dust fit over the whole temperature spectrum. By contrast, the CFDC and IS

plume n_s values are within an order of magnitude of the clean marine n_s fit. The WE-CAN data are also strikingly similar to the surface area normalized data for wildfire produced black carbon INPs reported by Schill et al. (2020) on the basis of ground-based plume measurements. Additionally, using data from the wildfire reported in Schill et al. (2020) that was previously only used to estimate black carbon INP n_s values, we have calculated the total n_s (all INPs) from these plume measurements (green diamonds in Figure 4b; Figure S6). The new total n_s calculations for the Pioneer Wildfire near Boise, Idaho, in August 2016 (Schill et al., 2020) used total reported INP concentrations and aerodynamic particle size measurements to encapsulate accumulation and coarse mode surface area for the IS measurement periods. In doing so, spherical

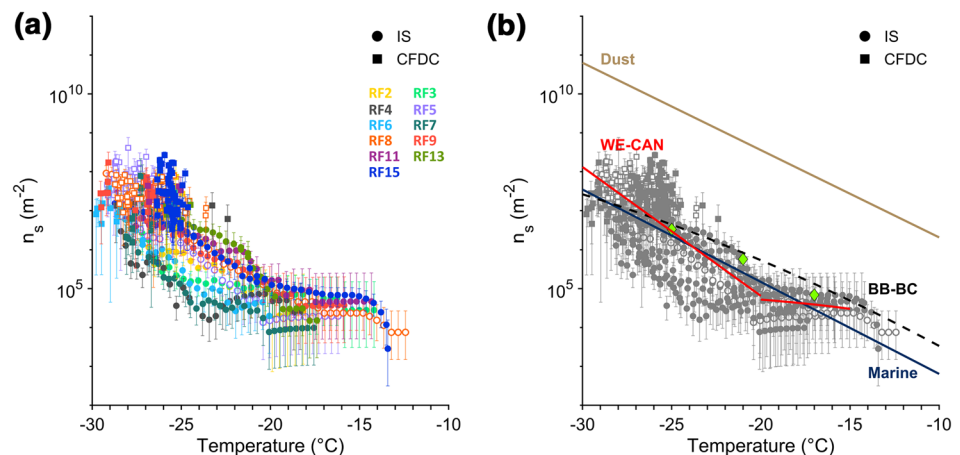


Figure 4. n_s for plume CFDC and IS data (a) colored by research flight (RF: Table 1) and (b) with an empirical fit to the data and comparison to previous fits for clean marine samples (McCluskey et al., 2018), black carbon from biomass burning (Schill et al., 2020) and desert dust (Ullrich et al., 2017). Aged smoke cases are shown as open circles. Green diamonds in (b) are new calculations of n_s for total smoke INPs measured at ground level for an August 2016 wildfire near Boise, ID reported in Schill et al. (2020). INP, ice-nucleating particle.

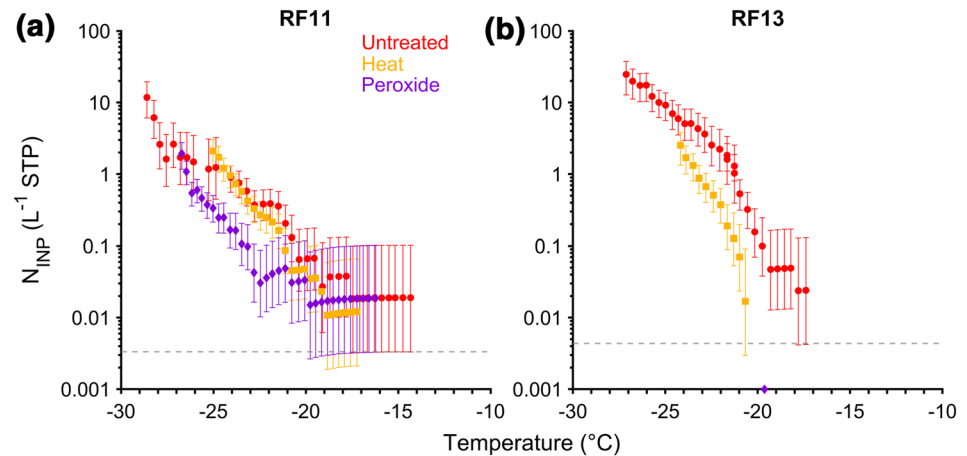


Figure 5. INP-temperature spectra showing changes after heat and peroxide treatments for (a) RF11 and (b) RF13. Dashed gray lines indicate the IS limit of detection. Points that were detected before field blank correction are given a value of 0.001 L^{-1} . Complete destruction of detectable INPs following peroxide digestion occurred for the RF13 sample. INP, ice-nucleating particle; IS, Ice Spectrometer.

particles of an effective density of 1.3 g cm^{-3} were assumed for conversion to physical diameters, and the distributions were then fit with lognormal functions. This reveals strong consistency of total biomass burning INP emissions (on a surface active site density basis) between the ground-based measurements and the new free tropospheric data in WE-CAN, for similar regions of the Western United States. Normalizing the data by surface area also highlights the aged smoke flights (RF5 and RF8) as relatively efficient sources of INPs from biomass burning, in contrast to some of the fresher, definable smoke plume passes (e.g., RF6 and RF7), which is evidence of the persistence of INPs in smoke away from the source. Combining the CFDC and IS n_s values from these 11 flights, we have fit an exponential to the plume data, $n_s (\text{m}^{-2}) = 0.016e^{-0.761T}$ for $-30 \leq T (\text{°C}) < -20$. Due to evidence of biological INPs at the warmer end of the temperature spectrum in several flights (Section 3.2), we have fit a linear function, $n_s (\text{m}^{-2}) = -4421T - 36,065$ for $-20 \leq T (\text{°C}) < -15$. These fits are shown in red in Figure 4b.

In addition to normalizing by surface area, dividing the INP concentrations by total number concentration allows comparisons to previous laboratory work in Levin et al. (2016) and Petters et al. (2009) by obtaining the activated fraction. Taking the logarithm of the activated fraction results in the ice nucleation efficiency parameter (ξ), which for WE-CAN, ranged from -5.9 to -4.4 at the average CFDC plume processing temperatures (-25.5°C to -29.2°C ; -26.6°C mean) given in Table 2. These ξ values are higher than values found at -30°C in laboratory burns of ponderosa pine branches (with needles) in Levin et al. (2016) ($\xi = -7$ to -6), and below the range of -4.2 to -3.3 in the 5 of 16 burns that exceeded the lower detection limit (-5.60 ± 0.6 average) of ponderosa pine needles in Petters et al. (2009). Thus, the in-plume measurements of ξ aloft are within the range of previous laboratory studies of INP emissions from a typical Western US fuel. However, data collected herein were for higher processing temperatures, and on the basis of slope of the INP temperature spectra, we can estimate that had we been able to evaluate ξ at -30°C , values would have been up to an order of magnitude higher. By inference then, the WE-CAN data predict a range of values at -30°C that meet the INP efficiency criteria for regional significance ($\xi = -4$ at -30°C) as outlined in Petters et al. (2009). Both definable (RF7: Donnell Fire) and sampled regional free-tropospheric (RF5: River of Smoke) plumes are most consistent with this conclusion, with average ξ of -4.4 (at -27.5°C) and -5 (at -27.4°C), respectively.

3.2. Composition of INPs in the Plume From the IS

Extracts from four plume filter samples were heated to detect the presence of biological INPs, and seven plume filter samples were subjected to peroxide digestion to remove all organic INPs; example spectra for two flights, RF11 and RF13, are shown in Figure 5 (other treatment spectra are shown in Figure S5). In the

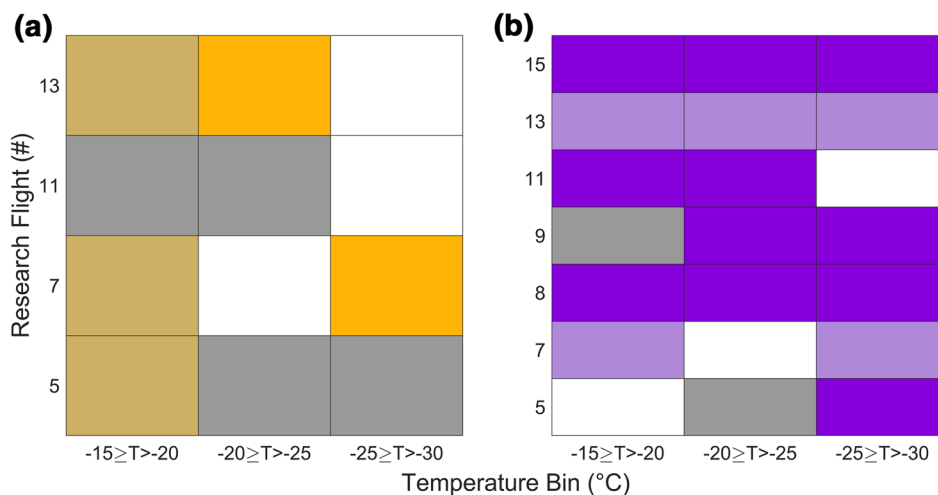


Figure 6. Heatmap indicating results of statistical significance tests for differences between untreated and (a) heat and (b) peroxide treated IS filters. Yellow and dark purple represent an increase of the untreated over the treated filter at 95% confidence, tan and light purple represent an increase over the treated filter with the treated measurement below the IS detection limit, gray represents no difference at 95% confidence, and white indicates missing data. IS, Ice Spectrometer.

samples from RF11, heat had no impact on the INP temperature spectrum, whereas in the RF13 sample, there was about a 5-fold decrease for processing temperatures above -23°C after heat treatment, indicating the presence of a biological INP population. Peroxide digestion decreased both spectra (no detectable INPs remained in the RF13 sample) indicating a predominance of organic INPs. Heatmap representations of the results from treatments (Figure 6) corroborate the observation of a heat impact only in some plumes and some temperature ranges, while peroxide digestion leads to a decrease in INPs, often in all temperature bins, in all samples. Three out of the four heat treated filters no longer had INP concentrations above the IS limit of detection in the highest temperature bin, consistent with the importance of biological INPs at higher temperatures. The results indicate that wildfire-derived INPs can sometimes be of biological origin, but the biological fraction is variable and a function of temperature. In contrast, organic INPs often comprised a major proportion of the total at the lowest part of the temperature spectrum, where mineral INPs are generally thought to dominate, at least for ambient atmospheric INPs (Murray et al., 2012). However, the ratio of organic to inorganic INPs is somewhat temperature and fire dependent. Our findings do not indicate that pure mineral INPs were absent, but rather that their overall fraction was small in these samples, consistent with the low n_s values observed everywhere in the free troposphere during WE-CAN. Additionally, this finding is consistent with the dominant organic INP fraction found in ground-based wildfire plume sampling in Schill et al. (2020). INPs from local soils cannot be ruled out, as they have been shown to contain abundant organic INPs (Hill et al., 2016; Tobo et al., 2014). Wood ash is a potential inorganic source of INPs (Grawe et al., 2016; Umo et al., 2015). Similar n_s values to the WE-CAN plumes were found in these laboratory studies using 0.1 wt% aqueous ash suspensions ($4.3 \times 10^5 \text{ m}^{-2}$ at -20°C). Nevertheless, the potential influence of this particle type appears secondary given the dominant organic INP population inferred from the IS data, for the particle size range collected in the aircraft measurements.

3.3. Case Study: South Sugarloaf Fire (RF15)

The sampling design for RF15 included multiple cross-plume transects at several altitudes, resulting in the most comprehensive CFDC and IS filter sampling of the study. The predominant fuel type burned was sagebrush shrubland, with aspen forest interspersed. The CFDC captured the highest absolute mean INP concentrations from the entire campaign in RF15. While the highest total particle number concentrations (10 nm–2.5 μm diameter) were observed closest to the source (Figure 7a), the CFDC measured the highest INP values some distance downwind of the fire (Figure 7b), representing samples with greater physical

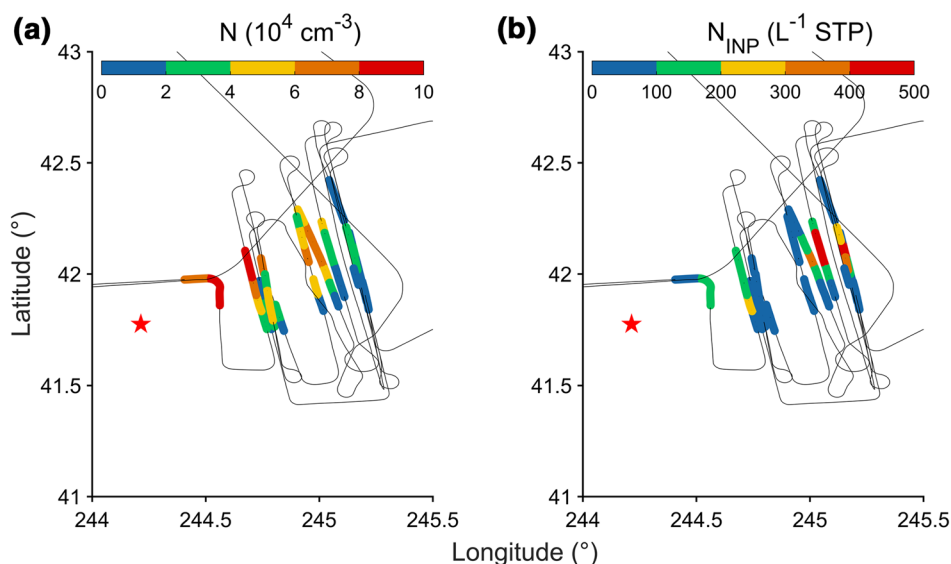


Figure 7. Flight track for the portion of RF15 that sampled the South Sugarloaf Fire over Nevada. The track is colored by in-plume (a) total particle number and (b) CFDC INP concentrations. The red star indicates the fire center. CFDC, Continuous Flow Diffusion Chamber; INP, ice-nucleating particle.

plume ages of 1–2 h. The INP concentrations also exhibited cross-plume variability, with the highest values measured in the center of the plume (upwards of 500 L^{-1} at -26°C). Elevated concentrations in a region of the plume with emissions exposed to longer atmospheric processing times may be attributable to a number of factors such as variability in emissions (since plume passes during this flight did not necessarily represent the same emission time window) or secondary production of particles active as INPs (explored in Section 3.3.1).

The South Sugarloaf Fire had a distinct population of in-plume INPs active at temperatures higher than about -20°C , with dissimilar (both in shape and magnitude) spectra in comparison to the out-of-plume background (Figure 8). While INPs active at temperatures warmer than -20°C were commonly seen in plumes sampled during WE-CAN, this filter had the sharpest increase in warm-temperature INP concentrations, which suggests a strong biological INP presence (Hill et al., 2018), although there was not enough sample for heat treatment. There was a large organic INP population over the entire plume temperature spectrum based on decreases in INP concentration after peroxide digestion (Figure 8). For example, there is over a 10-fold reduction in INPs at -25°C . Inorganic INPs show higher contributions below about -27°C . Peroxide digestion on the out-of-plume background also indicates some presence of organic INPs, which is not surprising given the abundance of aged biomass in the free troposphere, but this INP type contributes a smaller proportion (generally only a 2–3-fold decrease) across all temperatures.

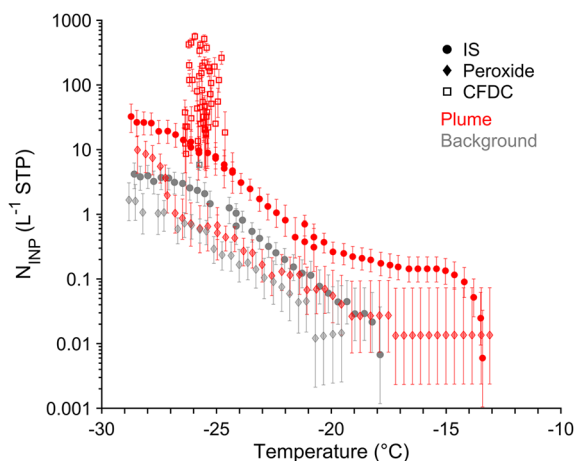


Figure 8. INP concentrations from the South Sugarloaf Fire (RF15) for the CFDC and IS, showing plume and out-of-plume background, and results after peroxide digestion on each filter suspension. CFDC, Continuous Flow Diffusion Chamber; INP, ice-nucleating particle; IS, Ice Spectrometer.

3.3.1. STEM Composition of Aerosol and INPs From the Plume

Two aerosol grids (RF15-A2 and RF15-C2) were collected to measure particles $<0.5 \mu\text{m}$ physical diameter from the fresher and aged parts of the plume, respectively, while one INP grid was collected over the whole plume sampling period to capture as many ice crystal residuals as possible. Analyses of the two aerosol grids were combined for comparison to the INP compositions. The RF15 physical plume ages sampled by the CFDC ranged from approximately 30 min to 2 h (mean 78 min), while

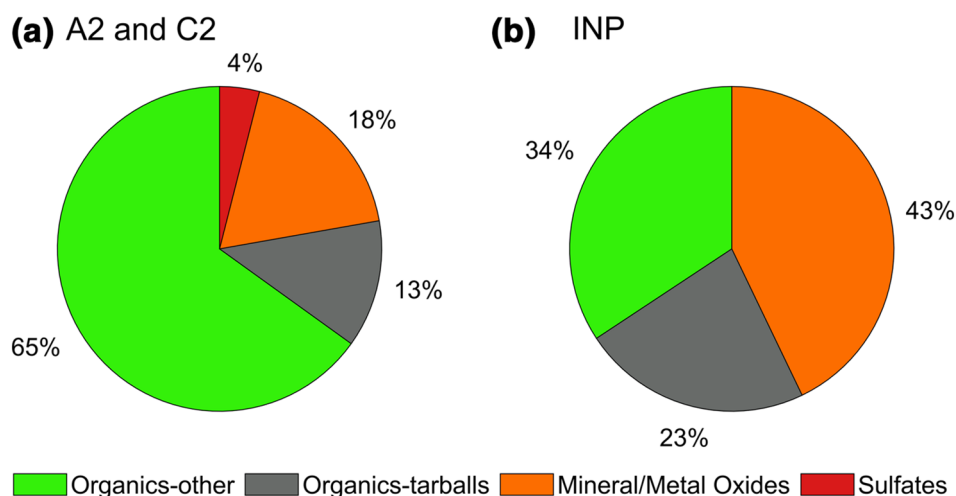


Figure 9. (a) Plume ambient aerosol and (b) plume INP particle categorization from STEM/EDX analysis for the South Sugarloaf Fire (RF15). Plume INPs were limited to those <0.5 microns in diameter to match the size of ambient particles collected on the second impactor stage. INP, ice-nucleating particle; IS, Ice Spectrometer; STEM/EDX, scanning transmission electron microscopy/energy dispersive X-ray spectroscopy.

the ambient samples had a mean plume age of 104 min. No attempt was made to calculate a representative average age, but the INP grid sample might be expected to be dominated by the higher INP concentrations found at longer aging times (Figure 7b). From the STEM/EDX analysis, 43 INPs (35 after setting <500 nm restriction) and 126 aerosol particles (combining RF15-A2 and RF15-C2) were categorized (Figure 9). Soot was a minor component by mass and number in these plumes (only 2 out of 517 total ambient particles from WE-CAN analyzed were so identified) and therefore are not included as a separate category.

Figure 9b reveals a majority (57%) of INPs in the plume are organic, with 23% of these categorized as tar balls. The mean diameter of all categorized INPs was 222 nm (for all INPs: 420 nm). The presence of tar balls as INPs from wildfires at the free-tropospheric level is consistent with their presence in ground-based samples, as reported by McCluskey et al. (2014), although the categorization used previously was based solely on particle composition and general morphology, and not on a roundness threshold as applied here. McCluskey et al. (2014) classified 67% of the INPs from the High Park Fire (collected for processing temperatures between -27°C and -30°C) as tar balls. Tar balls present as INPs indicate a secondary, plume-derived source, as they are thought to form by reactions of O and N with primary organic aerosol (Adachi et al., 2019). This results in a low volatility, high viscosity potential INP that we calculated as having a mean diameter of 218 nm, consistent with previous research (e.g., Adachi et al., 2019; Pósfai et al., 2004; Sedlacek et al., 2018). The percentage of tar balls found on the INP grid was enhanced compared with the combined A2 and C2 ambient grids. Tar balls could serve as a partial explanation for the enhanced INP concentrations found in many of the plume passes for RF15 that are most distant from the source (Figure 7). However, because the plane was not able to sample right next to the fire emissions source, even the closest passes (67 min physical plume age captured by the ambient RF15-A2 grid) had some indication of tar balls.

The dominance of organic INPs, with a still significant proportion of inorganics, found through STEM/EDX was consistent with the IS processing of the plume filter in the lower temperature region ($<-27^{\circ}\text{C}$; Figure 8). The ambient plume aerosol (Figure 9a) had a high organic influence (78%), while Mineral/Metal Oxides only comprised 18%, and thus, there was an INP enrichment of a little more than a factor of two for the inorganic category (at the average CFDC processing temperature of -25.6°C). Over coastal California, Cornwell et al. (2019) found an INP fraction of mineral dust of over 70% at a processing temperature of -31°C , contrasting with a mineral dust fraction of only 5% in the ambient particles (a factor of 14 enrichment). This indicates that the mineral particles found in the WE-CAN RF15 plume were not the dominant INP types except at the coldest temperatures, and enrichments as INPs compared to ambient particle mineral composition were modest (factor of 2). This is consistent with the CFDC n_s values of the plume being at least two orders of magnitude lower than the desert dust parameterization from Ullrich et al. (2017):

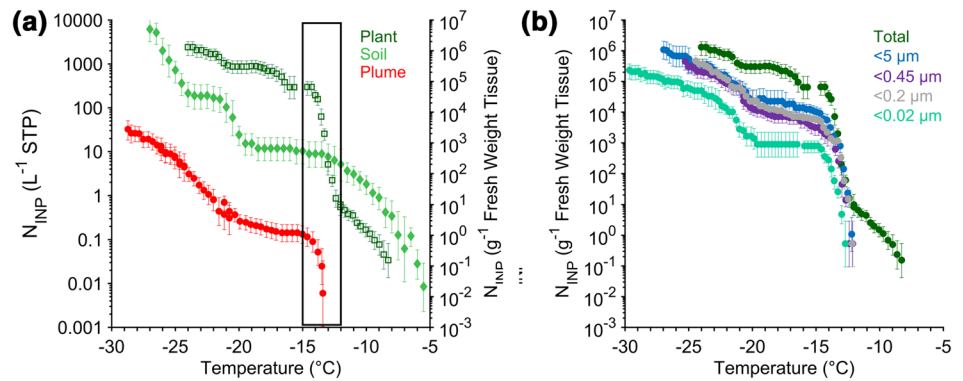


Figure 10. (a) INP concentrations from the (left axis) IS plume filter from the South Sugarloaf Fire, aerosolized sagebrush soil (Schiebel, 2017) and (right axis) aerosolized sagebrush tissue (plant). The black box highlights a comparison point of identical INP population onset temperature in the sagebrush tissue and South Sugarloaf plume sample. The sagebrush soil was sieved $< 75 \mu\text{m}$ and aerosolized in cloud chamber experiments with an average starting particle concentration of 154 cm^{-3} (Schiebel, 2017) before analysis with the IS; (b) Size fractionation of the aerosolized sagebrush tissue. INP, ice-nucleating particle; IS, Ice Spectrometer.

Average n_s from the RF15 plume passes was $4.6 \times 10^7 \text{ m}^{-2}$ (at the average CFDC plume processing temperature of -25.6°C), while the desert dust parameterization is $6.5 \times 10^9 \text{ m}^{-2}$ (at -25.6°C). As noted earlier, wood ash has been found to have comparably low n_s values, $3.4 \times 10^7 \text{ m}^{-2}$ (at -25.6°C) on the basis of parameterization of laboratory measurements (Umo et al., 2015). Particles comprising elements and morphologies typical of wood ash were tentatively identified as a minority of the inorganic in-plume INPs measured by STEM/EDX from the CFDC. These either had strong Mg and O signals, strong Ca (with S and O) signals, or a combination of these (e.g., Grawe et al., 2016). Such potential ash particles represented 7 of 43 total INPs analyzed, 16% of the overall INPs, and about 40% of the inorganic INP contributions measured at CFDC conditions.

3.3.2. Investigating Potential Origins of the INPs Sampled

We investigated the potential sources of the exceptionally abundant organic and, presumably, biological INPs in the South Sugarloaf Fire plume. In particular, we focused on the sagebrush fuel and the soil as sources of lofted INPs. Aerosolized sagebrush soil (Schiebel, 2017) and sagebrush plant tissue (Hill et al., 2016) samples from this ecotype have previously been tested for their INP properties. To compare with previous work and to understand the influence of INPs released from the plant in turbulence, sagebrush (*Artemisia tridentata*) leaf clippings were obtained from approximately 30 different shrubs at the same location (Jelm, WY) from which the soil and tissue samples were previously taken.

The clippings were shaken for 5 min in a one gallon plastic slider bag and then removed; dry-dislodged plant matter remaining in the bag (after waiting 10 min for settling) was suspended in 20 mL DI water for testing with the IS. Figure 10a shows striking similarities between the INP-temperature spectra from the aerosolized sagebrush tissue collected in Wyoming and that collected from the RF15 aircraft filter. In particular, they both have a rapid increase in INP concentration between -13°C and -14°C , with nearly identical slopes, indicating INP populations active at the same temperature. This increase is not present in the aerosolized soil dust, which has a much shallower slope at this temperature. The aerosolized sagebrush tissue ($> 5 \mu\text{m}$) additionally has another population of INPs at temperatures warmer than -13°C (Figure 10b) not seen in the WE-CAN data, likely due to the limit of detection of the IS (with lower aerial concentrations) combined with low efficiency in capturing larger particles through the aircraft inlet (Table S2). These results suggest the potential of lofted INPs from the sagebrush tissue itself, as Hill et al. (2016) measured a large increase in INP concentration at a similar temperature in both shoot and root tissues of sagebrush. This finding does not mean that the soil and other sagebrush ecotype fuels, such as various plants or litter (in addition to the other fuels burned), that were also consumed in the fire had no impact, but rather that

sagebrush tissue itself may have been the largest source of warm temperature ($>-15^{\circ}\text{C}$) INPs lofted into the plume. Moreover, Figure 10b indicates that 7.5% of the sagebrush tissue INPs at -20°C are smaller than $0.2\ \mu\text{m}$ and thus would be able to persist in the smoke plume and be sampled by the aircraft downwind of the fire center.

4. Conclusions

The WE-CAN campaign sampled many wildfire plumes across the western United States over the course of July–August 2018 and provided the first opportunity to quantify INPs within wildfire smoke plumes lofted into the free troposphere. We found a consistent enhancement of up to two orders of magnitude of INPs in-plume compared with corresponding out-of-plume background air, though variability existed among fires (Tables 2 and 3). Complicating the picture, the IS revealed some plumes (e.g., RF9 and RF13) had increases in concentrations only in portions of the temperature spectrum, indicating that only specific INP populations are enhanced in those cases (Figure 3). The IS and CFDC both showed that plumes are enhanced in INPs over the background air in most cases; however, the two approaches often produced divergent results in heterogeneous fresh plumes as opposed to the more uniform aged smoke, which was largely attributable to integration times.

The composition of the plume INPs were largely organic, even down to the lowest temperatures, with a secondary mineral influence (Figures 5 and 6). Moreover, some of the organic INPs may have been formed through secondary processing, as shown by the presence of tar balls in the South Sugarloaf Fire (RF15; Figure 9). Twenty-three percent of the INPs examined using STEM/EDX were tar balls. The very high INP concentrations (more than $500\ \text{L}^{-1}$ at $\sim -26^{\circ}\text{C}$) measured in this plume, primarily downwind, could partly be explained through such in-plume INP production. Though tar balls were also seen in ground-based wildfire sampling in McCluskey et al. (2014), this is the first evidence of activity as INPs at cloud altitudes. The ubiquity of tar balls as INPs in smoke from different fuel and fire types remains an open question.

Material of biological origin was found to be a potential in-plume INP, as evidenced from heat treatment of several filter suspensions (Figures 5 and 6). This finding supports the idea that wildfires loft uncombusted material from a zone of turbulence surrounding the fire center (Wagner et al., 2018). RF15 sampled a plume from burning of a predominantly sagebrush fuel. Comparison of its INP temperature spectrum with those obtained from sagebrush soil dust (Schiebel, 2017) and dry-dislodged sagebrush leaf clippings suggest the sagebrush tissue itself as the most likely source of INPs measured in RF15 within the temperature range accessible for the limits of detection for our measurement methods, rather than soil or the microbiota of the phyllosphere (Figure 10a). A sizable fraction of these INPs was also smaller than $0.2\ \mu\text{m}$, which is important as these particles can remain airborne during long range plume transport (Figure 10b).

Modeling the role of INPs from wildfires is critical for assessing climate impacts. The consistent increase of INPs in plume relative to the background free troposphere, despite smoke not being an especially efficient source on the basis of low n_s values, suggests it has the potential to modify cloud glaciation and precipitation downwind. Since these are the first reported free-tropospheric INP measurements from wildfires, more data will be needed to solidify these findings and verify the trends for implementation in models. However, it is encouraging to find consistency with previous ground- and laboratory-based work regarding Western US wildfire fuels, including a dominant organic INP composition (Schill et al., 2020), presence of tar balls in INP samples (McCluskey et al., 2014), lack of a major contribution to INPs from black carbon particles (McCluskey et al., 2014; Levin et al., 2016; Schill et al., 2020), and INP fractions with respect to total particle numbers generated that span the range found in prior laboratory studies (Petters et al., 2009; Levin et al., 2016) and appear in many cases to meet the criteria for regional significance established in Petters et al. (2009). The exact role of the fuel type and combustion conditions in relation to INP plume enhancement remains unclear as each wildfire burns multiple fuels, which limits generalizations. Nevertheless, this study shows that wildfire smoke INPs persist in diluting plumes, have local and sometimes regional significance in determining free tropospheric INP concentrations, and are therefore relevant to understanding future impacts on clouds in a climate with more wildfires.

Data Availability Statement

The data that support the findings of this study are available from https://data.eol.ucar.edu/master_lists/generated/we-can/.

Acknowledgments

This work was supported by the National Science Foundation, Award #AGS-1650786, AGS-1650288, AGS-1433517, and NOAA Climate Program Office's Atmospheric Chemistry, Carbon Cycle, and Climate program grant NA17OAR4310010. Kathryn A. Moore acknowledges support by a National Science Foundation Graduate Research Fellowship under Grant No. 006784. The authors thank the entire WE-CAN team and the US Forest Service team for identification of plume locations, times, and fuel types. Thanks to Bryan Rainwater, Stephanie Redfern, and Adriana Bailey for assistance in the field collecting impactor samples. Special thanks to Thea Schiebel for sharing data from her dissertation for use in Figure 10. Additionally, thank you to the three anonymous reviewers whose insights greatly improved this manuscript.

References

- Adachi, K., Sedlacek, A. J., Kleinman, L., Springston, S. R., Wang, J., Chand, D., et al. (2019). Spherical tar ball particles form through rapid chemical and physical changes of organic matter in biomass-burning smoke. *Proceedings of the National Academy of Sciences of the United States of America*, *116*, 19336–19341. <https://doi.org/10.1073/PNAS.1900129116>
- Agresti, A., & Coull, B. A. (1998). Approximate is better than “exact” for interval estimation of binomial proportions. *The American Statistician*, *52*, 119–126. <https://doi.org/10.2307/2685469>
- Brey, S. J., Barnes, E. A., Pierce, J. R., Swann, A. L. S., & Fischer, E. V. (2020). Past variance and future projections of the environmental conditions driving western U.S. summertime wildfire burn area. *Earth's Future*, *8*, 1745–1761. <https://doi.org/10.1029/2020EF001645>
- Clarke, A. D., Shinozuka, Y., Kapustin, V. N., Howell, S., Huebert, B., Doherty, S., et al. (2004). Size distributions and mixtures of dust and black carbon aerosol in Asian outflow: Physiochemistry and optical properties. *Journal of Geophysical Research*, *109*(D15), D15S09. <https://doi.org/10.1029/2003JD004378>
- Cornwell, G. C., McCluskey, C. S., Levin, E. J. T., Suski, K. J., DeMott, P. J., Kreidenweis, S. M., et al. (2019). Direct online mass spectrometry measurements of ice nucleating particles at a California Coastal Site. *Journal of Geophysical Research: Atmosphere*, *124*, 12157–12172. <https://doi.org/10.1029/2019JD030466>
- DeMott, P. J. (1995). Quantitative descriptions of ice formation mechanisms of silver iodide, type aerosols. *Atmospheric Research*, *38*, 63–99. [https://doi.org/10.1016/0169-8095\(94\)00088-U](https://doi.org/10.1016/0169-8095(94)00088-U)
- DeMott, P. J., Hill, T. C. J., Petters, M. D., Bertram, A. K., Tobo, Y., Mason, R. H., et al. (2017). Comparative measurements of ambient atmospheric concentrations of ice nucleating particles using multiple immersion freezing methods and a continuous flow diffusion chamber. *Atmospheric Chemistry and Physics*, *17*, 11227–11245. <https://doi.org/10.5194/ACP-17-11227-2017>
- DeMott, P. J., Möhler, O., Cziczo, D. J., Hiranuma, N., Petters, M. D., Petters, S. S., et al. (2018). The Fifth International Workshop on Ice Nucleation phase 2 (FIN-02): Laboratory intercomparison of ice nucleation measurements. *Atmospheric Measurement Techniques*, *11*, 6231–6257. <https://doi.org/10.5194/AMT-11-6231-2018>
- DeMott, P. J., Prenni, A. J., Liu, X., Kreidenweis, S. M., Petters, M. D., Twohy, C. H., et al. (2010). Predicting global atmospheric ice nuclei distributions and their impacts on climate. *Proceedings of the National Academy of Sciences of the United States of America*, *107*, 11217–11222. <https://doi.org/10.1073/PNAS.0910818107>
- DeMott, P. J., Prenni, A. J., McMeeking, G. R., Sullivan, R. C., Petters, M. D., Tobo, Y., et al. (2015). Integrating laboratory and field data to quantify the immersion freezing ice nucleation activity of mineral dust particles. *Atmospheric Chemistry and Physics*, *15*, 393–409. <https://doi.org/10.5194/ACP-15-393-2015>
- Flannigan, M. D., Krawchuk, M. A., de Groot, W. J., Mike Wotton, B., & Gowman, L. M. (2009). Implications of changing climate for global wildland fire. *International Journal of Wildland Fire*, *18*, 483–507. <https://doi.org/10.1071/WF08187>
- Garofalo, L. A., Pothier, M. A., Levin, E. J. T., Campos, T., Kreidenweis, S. M., & Farmer, D. K. (2019). Emission and evolution of submicron organic aerosol in smoke from wildfires in the Western United States. *ACS Earth and Space Chemistry*, *3*, 1237–1247. <https://doi.org/10.1021/ACSEARTHSPACECHEM.9B00125>
- Grawe, S., Augustin-Bauditz, S., Hartmann, S., Hellner, L., Pettersson, J. B. C., Prager, A., et al. (2016). The immersion freezing behavior of ash particles from wood and brown coal burning. *Atmospheric Chemistry and Physics*, *16*, 13911–13928. <https://doi.org/10.5194/ACP-16-13911-2016>
- Hill, T. C. J., DeMott, P. J., Conen, F., & Möhler, O. (2018). Impacts of bio aerosols on atmospheric ice nucleation processes. In A.-M. Delort, & P. Amato (Eds.), *Microbiology of aerosols* (1st ed., pp. 197–219). Hoboken, NJ: John Wiley & Sons. <https://doi.org/10.1002/9781119132318>
- Hill, T. C. J., DeMott, P. J., Tobo, Y., Fröhlich-Nowoisky, J., Moffett, B. F., Franc, G. D., et al. (2016). Sources of organic ice nucleating particles in soils. *Atmospheric Chemistry and Physics*, *16*, 7195–7211. <https://doi.org/10.5194/ACP-16-7195-2016>
- Huebert, B. J., Howell, S. G., Covert, D. S., Bertram, T., Clarke, A. D., Anderson, J. R., et al. (2004). PELTI: Measuring the passing efficiency of an airborne low turbulence aerosol inlet. *Aerosol Science and Technology*, *38*, 803–826. <https://doi.org/10.1080/027868290500823>
- Kanji, Z. A., Ladino, L. A., Wex, H., Boose, Y., Burkert-Kohn, M., Cziczo, D. J., et al. (2017). Overview of ice nucleating particles. *Meteorological Monographs*, *58*, 1–33. <https://doi.org/10.1175/AMSMONOGRAPHIS-D-16-0006.1>
- Kupc, A., Williamson, C., Wagner, N. L., Richardson, M., & Brock, C. A. (2018). Modification, calibration, and performance of the ultra-high sensitivity aerosol spectrometer for particle size distribution and volatility measurements during the atmospheric tomography mission (atom) airborne campaign. *Atmospheric Measurement Techniques*, *11*, 369–383. <https://doi.org/10.5194/AMT-11-369-2018>
- Lebague, B., Schmidt, M., Ramonet, M., Wastine, B., Kwok, C. Y., Laurent, O., et al. (2016). Comparison of nitrous oxide (N₂O) analyzers for high-precision measurements of atmospheric mole fractions. *Atmospheric Measurement Techniques*, *9*, 1221–1238. <https://doi.org/10.5194/AMT-9-1221-2016>
- Levin, E. J. T., DeMott, P. J., Suski, K. J., Boose, Y., Hill, T. C. J., McCluskey, C. S., et al. (2019). Characteristics of ice nucleating particles in and around California winter storms. *Journal of Geophysical Research: Atmosphere*, *124*, 11530–11551. <https://doi.org/10.1029/2019JD030831>
- Levin, E. J. T., McMeeking, G. R., DeMott, P. J., McCluskey, C. S., Carrico, C. M., Nakao, S., et al. (2016). Ice-nucleating particle emissions from biomass combustion and the potential importance of soot aerosol. *Journal of Geophysical Research: Atmosphere*, *121*, 5888–5903. <https://doi.org/10.1002/2016JD024879>
- Liu, J. C., Mickley, L. J., Sulprizio, M. P., Dominici, F., Yue, X., Ebisu, K., et al. (2016). Particulate air pollution from wildfires in the Western US under climate change. *Climatic Change*, *138*, 655–666. <https://doi.org/10.1007/S10584-016-1762-6>
- Lohmann, U. (2002). A glaciation indirect aerosol effect caused by soot aerosols. *Geophysical Research Letters*, *29*, 1052. <https://doi.org/10.1029/2001GL014357>
- McClure, C. D., & Jaffe, D. A. (2018). US particulate matter air quality improves except in wildfire-prone areas. *Proceedings of the National Academy of Sciences of the United States of America*, *115*, 7901–7906. <https://doi.org/10.1073/PNAS.1804353115>
- McCluskey, C. S., DeMott, P. J., Prenni, A. J., Levin, E. J. T., McMeeking, G. R., Sullivan, A. P., et al. (2014). Characteristics of atmospheric ice nucleating particles associated with biomass burning in the US: Prescribed burns and wildfires. *Journal of Geophysical Research: Atmosphere*, *119*, 10458–10470. <https://doi.org/10.1002/2014JD021980>

- McCluskey, C. S., Ovadnevaite, J., Rinaldi, M., Atkinson, J., Belosi, F., Ceburnis, D., et al. (2018). Marine and terrestrial organic ice-nucleating particles in Pristine Marine to continentally influenced Northeast Atlantic air masses. *Journal of Geophysical Research: Atmosphere*, *123*, 6196–6212. <https://doi.org/10.1029/2017JD028033>
- Mültenstädt, J., Sourdeval, O., Delanoë, J., & Quaas, J. (2015). Frequency of occurrence of rain from liquid-, mixed-, and ice-phase clouds derived from A-Train satellite retrievals. *Geophysical Research Letters*, *42*, 6502–6509. <https://doi.org/10.1002/2015GL064604>
- Murray, B. J., O'Sullivan, D., Atkinson, J. D., & Webb, M. E. (2012). Ice nucleation by particles immersed in supercooled cloud droplets. *Chemical Society Reviews*, *41*, 6519. <https://doi.org/10.1039/C2CS35200A>
- Niemand, M., Möhler, O., Vogel, B., Vogel, H., Hoose, C., Connolly, P., et al. (2012). A particle-surface-area-based parameterization of immersion freezing on desert dust particles. *Journal of the Atmospheric Sciences*, *69*, 3077–3092. <https://doi.org/10.1175/JAS-D-11-0249.1>
- O'Dell, K., Ford, B., Fischer, E. V., & Pierce, J. R. (2019). The contribution of wildland-fire smoke to US PM_{2.5} and its influence on recent trends. *Environmental Science and Technology*, *53*, 1797–1804. <https://doi.org/10.1021/ACS.EST.8B05430>
- Petters, M. D., Parsons, M. T., Prenni, A. J., DeMott, P. J., Kreidenweis, S. M., Carrico, C. M., et al. (2009). Ice nuclei emissions from biomass burning. *Journal of Geophysical Research*, *114*, D07209. <https://doi.org/10.1029/2008JD011532>
- Pósfai, M., Gelencsér, A., Simonics, R., Arató, K., Li, J., Hobbs, P. V., et al. (2004). Atmospheric tar balls: Particles from biomass and biofuel burning. *Journal of Geophysical Research*, *109*, D06213. <https://doi.org/10.1029/2003JD004169>
- Prenni, A. J., DeMott, P. J., Sullivan, A. P., Sullivan, R. C., Kreidenweis, S. M., & Rogers, D. C. (2012). Biomass burning as a potential source for atmospheric ice nuclei: Western wildfires and prescribed burns. *Geophysical Research Letters*, *39*, L11805. <https://doi.org/10.1029/2012GL051915>
- Rogers, D. C. (1988). Development of a continuous flow thermal gradient diffusion chamber for ice nucleation studies. *Atmospheric Research*, *22*, 149–181. [https://doi.org/10.1016/0169-8095\(88\)90005-1](https://doi.org/10.1016/0169-8095(88)90005-1)
- Rogers, D. C., DeMott, P. J., & Kreidenweis, S. M. (2001). Airborne measurements of tropospheric ice-nucleating aerosol particles in the Arctic spring. *Journal of Geophysical Research*, *106*, 15053–15063. <https://doi.org/10.1029/2000JD900790>
- Schiebel, T. (2017). *Ice nucleation activity of soil dust aerosols*. Karlsruhe, Germany: Karlsruhe Institute of Technology. <https://doi.org/10.5445/IR/1000076327>
- Schill, G. P., DeMott, P. J., Emerson, E. W., Rauker, A. C., Kodros, J. K., Suski, K. J., et al. (2020). The contribution of black carbon to global ice nucleating particle concentrations relevant to mixed-phase clouds. *Proceedings of the National Academy of Sciences of the United States of America*, *117*, 22705–22711. <https://doi.org/10.1073/PNAS.2001674117>
- Sedlacek, A. J., III, Buseck, P. R., Adachi, K., Onasch, T. B., Springston, S. R., & Kleinman, L. (2018). Formation and evolution of tar balls from northwestern US wildfires. *Atmospheric Chemistry and Physics*, *18*, 11289–11301. <https://doi.org/10.5194/ACP-18-11289-2018>
- Spracklen, D. V., Mickley, L. J., Logan, J. A., Hudman, R. C., Yevich, R., Flannigan, M. D., et al. (2009). Impacts of climate change from 2000 to 2050 on wildfire activity and carbonaceous aerosol concentrations in the western United States. *Journal of Geophysical Research*, *114*, D20301. <https://doi.org/10.1029/2008JD010966>
- Suski, K. J., Hill, T. C. J., Levin, E. J. T., Miller, A., DeMott, P. J., & Kreidenweis, S. M. (2018). Agricultural harvesting emissions of ice-nucleating particles. *Atmospheric Chemistry and Physics*, *18*, 13755–13771. <https://doi.org/10.5194/ACP-18-13755-2018>
- Tobo, Y., DeMott, P. J., Hill, T. C. J., Prenni, A. J., Swoboda-Colberg, N. G., Franc, G. D., et al. (2014). Organic matter matters for ice nuclei of agricultural soil origin. *Atmospheric Chemistry and Physics*, *14*, 8521–8531. <https://doi.org/10.5194/ACP-14-8521-2014>
- Ullrich, R., Hoose, C., Niemand, M., Wagner, R., Höhler, K., et al. (2017). A new ice nucleation active site parameterization for desert dust and soot. *Journal of the Atmospheric Sciences*, *74*, 699–717. <https://doi.org/10.1175/JAS-D-16-0074.1>
- Umo, N. S., Murray, B. J., Baeza-Romero, M. T., Jones, J. M., Lea-Langton, A. R., Malkin, T. L., et al. (2015). Ice nucleation by combustion ash particles at conditions relevant to mixed-phase clouds. *Atmospheric Chemistry and Physics*, *15*, 5195–5210. <https://doi.org/10.5194/ACP-15-5195-2015>
- Vali, G. (1971). Quantitative evaluation of experimental results and the heterogeneous freezing nucleation of super cooled liquids. *Journal of the Atmospheric Sciences*, *28*, 402–409. [https://doi.org/10.1175/1520-0469\(1971\)028<0402:QEOERA>2.0.CO;2](https://doi.org/10.1175/1520-0469(1971)028<0402:QEOERA>2.0.CO;2)
- Wagner, R., Jähn, M., & Schepanski, K. (2018). Wildfires as a source of airborne mineral dust – revisiting a conceptual model using large-eddy simulation (LES). *Atmospheric Chemistry and Physics*, *18*, 11863–11884. <https://doi.org/10.5194/ACP-18-11863-2018>
- Westerling, L., Turner, M. G., Smithwick, E. A. H., Romme, W. H., & Ryan, M. G. (2011). Continued warming could transform Greater Yellowstone fire regimes by mid-21st century. *Proceedings of the National Academy of Sciences of the United States of America*, *108*, 13165–13170. <https://doi.org/10.1073/PNAS.1110199108>
- Yue, X., Mickley, L. J., Logan, J. A., & Kaplan, J. O. (2013). Ensemble projections of wildfire activity and carbonaceous aerosol concentrations over the western United States in the mid-21st century. *Atmospheric Environment*, *77*, 767–780. <https://doi.org/10.1016/J.ATMOENV.2013.06.003>

Reference From Supporting Information

- Krishnamoorthy, K., & Lee, M. (2012). New approximate confidence intervals for the difference between two Poisson means and comparison. *Journal of Statistical Computation and Simulation*, *83*, 2232–2243. <https://doi.org/10.1080/00949655.2012.686616>